APL Photonics

RESEARCH ARTICLE | NOVEMBER 12 2018

Invited Article: Ultra-broadband terahertz coherent detection via a silicon nitride-based deep sub-wavelength metallic slit

A. Tomasino; R. Piccoli; Y. Jestin; S. Delprat; M. Chaker; M. Peccianti ; M. Clerici ; A. Busacca; L. Razzari; R. Morandotti

APL Photonics 3, 110805 (2018)
https://doi.org/10.1063/1.5052628

Invited Article: Ultra-broadband terahertz coherent detection via a silicon nitride-based deep sub-wavelength metallic slit

A. Tomasino,[1,2] R. Piccoli,[1,a] Y. Jestin,[1] S. Delprat,[1] M. Chaker,[1]
M. Peccianti,[3] M. Clerici,[4] A. Busacca,[2] L. Razzari,[1] and R. Morandotti[1,5,6,b]
[1]*INRS-EMT, 1650 Boulevard Lionel-Boulet, Varennes, Québec J3X 1S2, Canada*
[2]*DEIM, University of Palermo, Viale delle Science Ed. 9, Palermo 90128, Italy*
[3]*Department of Physics and Astronomy, University of Sussex, Falmer, Brighton BN1 9RH, United Kingdom*
[4]*School of Engineering, University of Glasgow, Glasgow G12 8QQ, United Kingdom*
[5]*ITMO University, St. Petersburg 199034, Russia*
[6]*Institute of Fundamental and Frontier Sciences, University of Electronic Science and Technology of China, Chengdu 610054, Sichuan, China*

(Received 20 August 2018; accepted 23 October 2018; published online 12 November 2018)

We present a novel class of CMOS-compatible devices aimed to perform the solid-state-biased coherent detection of ultrashort terahertz pulses, i.e., featuring a gap-free bandwidth at least two decades-wide. Such a structure relies on a 1-μm-wide slit aperture located between two parallel aluminum pads, embedded in a 1-μm-thick layer of silicon nitride, and deposited on a quartz substrate. We show that this device can detect ultra-broadband terahertz pulses by employing unprecedented low optical probe energies of only a few tens of nanojoules. This is due to the more than one order of magnitude higher nonlinear coefficient of silicon nitride with respect to silica, the nonlinear material employed in the previous generations. In addition, due to the reduced distance between the aluminum pads, very high static electric fields can be generated within the slit by applying extremely low external bias voltages (in the order of few tens of volts), which strongly enhance the dynamic range of the detected THz waveforms. These results pave the way to the integration of solid-state ultra-broadband detection in compact and miniaturized terahertz systems fed by high repetition-rate laser oscillators and low-noise, low-voltage generators. https://doi.org/10.1063/1.5052628

I. INTRODUCTION

The realization of innovative techniques able to manage ultra-broadband terahertz (THz) pulses, i.e., electromagnetic waves, the spectra of which cover a two-decade wide frequency range (0.1-10 THz) or more,[1,2] has always been of particularly interest due to the advantages that such a wide spectral range brings about with respect to conventional THz systems.[3] Indeed, on the one hand, a 10 THz-wide radiation lasts only few hundreds of femtoseconds (full width at half maximum), enabling high-resolution time-of-flight measurements for, e.g., 3D THz imaging of multilayered structures[4] or thickness evaluation of thin films.[5,6] On the other hand, many materials, such as semiconductors,[7] liquid crystals,[8] chemicals like drugs and explosives,[9] as well as biopolymers like proteins and DNA,[10–12] possess specific roto/vibrational modes above 2 THz. Therefore, the possibility of providing ultra-broadband detection capabilities is essential for their complete investigation in a wider THz spectral window.[13] Until now the most common detection mechanisms are based on either

[a]Electronic mail: riccardo.piccoli@emt.inrs.ca
[b]Electronic mail: morandotti@emt.inrs.ca

electro-optic sampling (EOS) or photoconductive switches (PCSs), which address THz bandwidths typically smaller than 7 THz.[7,14–17] This is due to inherent limitations of the detection media, such as dispersion, absorption, long carrier lifetime, and lattice resonances.[18] Therefore, detection methods able to operate in the ultra-broadband regime are mainly gas-based, which enable spectral investigations up to or beyond 10 THz, assuming that the pulse duration of the employed ultrafast laser is sufficiently short. Gases are continuously renewed, do not show appreciable dispersion, and lack phonon resonances due to the absence of an ordered structure.[19] Among such schemes, it is worth mentioning air-breakdown coherent detection,[20] air-biased coherent detection[21] (ABCD), optically biased coherent detection,[22] and THz radiation enhanced emission of fluorescence.[23] In particular, ABCD exploits a third-order nonlinear process named electric-field-induced second harmonic (EFISH) generation. Here, the superposition of the THz radiation and a bias electric field breaks the symmetry of air and thus induces the frequency doubling of a propagating optical probe beam. Such a nonlinear mixing results in a total EFISH beam intensity containing a term directly proportional to the THz electric field. By modulating the bias electric field and performing heterodyne detection via a lock-in amplifier, it is possible to isolate and record such a linear term, thus reconstructing both amplitude and phase of the THz transient. Building on this detection approach, we achieved an important breakthrough, demonstrating an ultra-broadband detection scheme relying on the EFISH generation process in a thin film of UV fused silica, which we named solid-state biased coherent detection (SSBCD).[2] SSBCD requires up to three orders of magnitude lower probe energy (<1 μJ) and can achieve high dynamic ranges (DRs) by applying lower bias voltages (<500 V), due to the higher nonlinearity and breakdown voltage of silica with respect to air, together with a reduced width of the biased region. Moreover, it is fully compatible with CMOS processes, thus enabling miniaturization as well as the realization of cost-effective integrated devices. Despite the extremely promising results achieved with the first generation of SSBCD devices, there is still room for improvement to make the SSBCD technique competitive in those applications where EOS and PCS dominate.

Here, we present a new class of SSBCD detectors, based on a micron-size metallic slit, embedded in a thin film of silicon nitride (SiN), acting as the nonlinear medium. In such a configuration, we show that, despite the deep sub-wavelength (λ) width of the slit compared to THz wavelengths, the higher nonlinear coefficient of SiN [$\chi^{(3)} \sim 8 \times 10^{-21}$ m^2/V^2, more than one order of magnitude higher than that of silica[24]] allows for a remarkable ultra-broadband detection capability, now achieved by using extremely low bias voltages and probe pulse energies.

II. LAYOUT DESIGN AND DEVICE FABRICATION

The layout of the sub-λ SSBCD device is presented in Fig. 1 and essentially resembles the structure reported in Ref. 2. It consists of the deposition (on a 1.5-mm-thick fused quartz substrate) of a 30-nm-thick layer of chromium (Cr) followed by a 100-nm-thick layer of aluminum and another 30-nm-thick layer of Cr. Both the two Cr layers ensure the proper adhesion of the dielectric materials over the aluminum. Two electrodes are then defined by direct-write laser lithography and wet etching techniques, in order to form a 1.0 ± 0.1 μm-wide gap (G) between them. Subsequently, a 1-μm-thick SiN cover layer is deposited via plasma-enhanced chemical vapor deposition (PECVD) over part of the electrodes, thus also completely filling the slit. The cover layer thickness (T) was chosen according to previous simulations,[2] establishing that in order to prevent discharges induced by the high bias electric fields in the air above the dielectric material, its minimum size should be the same as the slit. The aluminum pad sizes were chosen as W = L = 2 mm. We fabricated a batch of twenty devices, all of them realized on the same quartz substrate. This ensured that the whole batch shared the same features, such as composition of the SiN layer and quality of the aluminum pads. Additionally, we would like to emphasize that the CMOS process employed here allows us to easily reproduce the properties of these structures with very high reliability.

We note that such a narrow slit features a specific spectral response, which we exploited as a further parameter to improve the overall detection efficiency. Indeed, when a THz wave is being funneled into a freestanding sub-λ metal slit, it gives rise to a carrier surface density, the fast transients of which induce accumulation of the carriers at the edges of the metal pads, thus enhancing the THz electric field within the slit.[25,26] The funneling effect through narrow slits was mostly investigated in

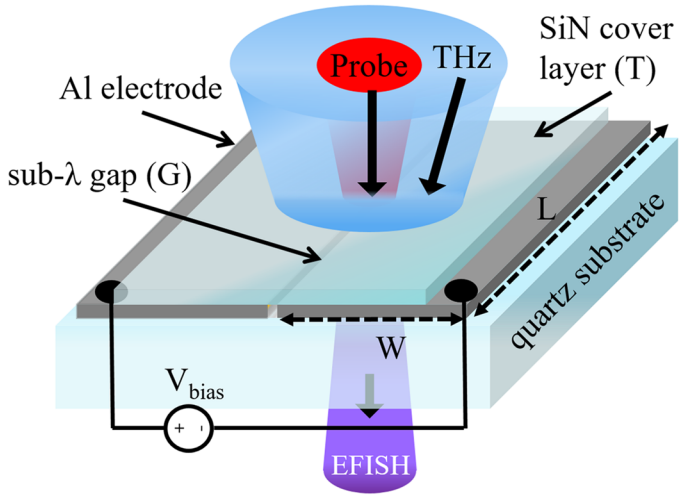

FIG. 1. 3D sketch of the deep sub-**λ** slit (G) device embedded in a thin layer (T) of SiN, deposited on a quartz substrate. L and W are the length and the width of the metal pads, respectively.

relatively low ranges of frequencies, mainly between 0.1 and 1.6 THz, where the field enhancement (FE) is the highest.[25–28] For our purpose, it is instead essential to study the behavior of the sub-λ slit in a much broader spectral window, under the hypothesis of a focusing THz beam. For these reasons, we performed simulations with the aid of a frequency-dependent finite element method-based software (COMSOL Multiphysics®), the details of which are explained in the supplementary material. The main outcomes of such an investigation are shown in Fig. 2. In particular, Fig. 2(a) depicts the 2D distribution of the THz electric field around the slit illuminated by a focusing beam at the frequency component of 5 THz, i.e., roughly at the center of the investigated range of 0.25-10 THz. Figure 2(b) shows the simulated FE as a function of the frequency overlapped to the bandwidth of the THz pulses emitted by our THz plasma source and acquired via ABCD (as detailed later in the text). Here, we recall that the FE is evaluated as the ratio between the THz electric field within the slit aperture and the background field, i.e., the field expected value in a plain layer of SiN without the surrounding metal pads. The frequency-weighted mean value of the FE is equal to 6.1. Incidentally, we note that the THz spectrum of our reference source does not show a significant low frequency content since the plasma cut-off frequency is around 1 THz, under our experimental conditions.[29] Therefore, the FE acting on the incident THz pulses results to be more effective at higher frequencies, where it only shows a slight frequency dependence. Hence, the THz bandwidth reconstructed via this new type

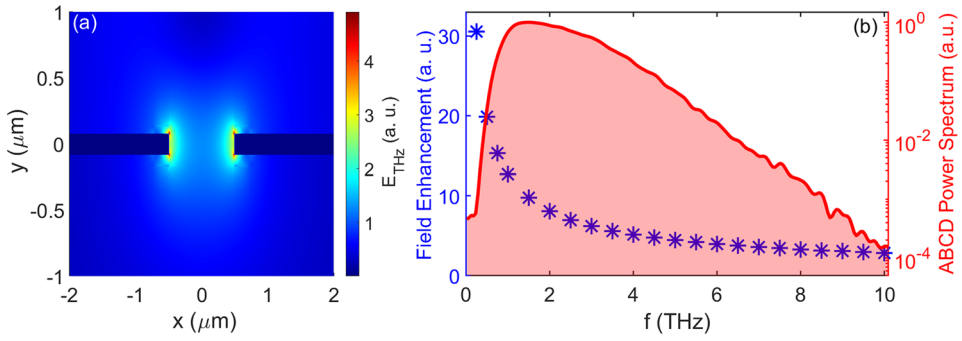

FIG. 2. Simulation of the field enhancement. (a) 2D norm of the THz electric field distributed around the slit for the frequency component of 5 THz. (b) Calculated field enhancement values (blue stars) induced by the metallic slit on a focusing ultra-broadband THz beam, as a function of the frequency, in the 0.25-10 THz range. The red area represents the THz spectrum emission from our two-color plasma source, acquired via the ABCD technique (details are given throughout the text).

of slit device is expected to be nearly the same of the one measured via ABCD, as experimentally verified below.

III. EXPERIMENTAL RESULTS

A. Comparison with the ABCD technique

We have preliminary tested three samples of the new detector type via an ultra-broadband THz-Time Domain Spectroscopy (TDS) system completely purged with nitrogen.[2] The experiments implied the use of a two-color plasma source driven by a 1 mJ, 800 nm, 140 fs, 1 kHz Ti:Sapphire pulsed laser, emitting THz pulses with a bandwidth exceeding 10 THz. We measured a THz peak value of 43.8 ± 1.2 kV/cm at the detector position, via EOS in a 500-μm-thick GaP crystal.[30] We started the characterization comparing the spectral response of the devices against standard ABCD, the latter being performed by focusing the THz and the 50-μJ-probe beam together in air through a 2-in.-parabolic mirror and a 100-mm-lens, respectively. In this way, while the THz spot size was frequency-dependent (with an average $1/e^2$-radius of 150 μm), the $1/e^2$-radius of the probe beam was fixed at approximately 10 μm, on the focal plane. For ABCD, we biased the interaction with a 2 kV AC (square wave) bias voltage at 500 Hz. For SSBCD, we kept the same focusing condition for both beams and decreased the probe energy to 100 nJ and the bias voltage to 100 V. Since the results achieved with the three devices were very similar (i.e., standard deviation lower than 4%), here we report, for the sake of simplicity, the data of one detector only. In particular, the waveforms acquired through both techniques are shown in Fig. 3, whereas the corresponding Fourier-transformed spectra are shown in the inset. Consistently with our simulations, the FE induced by the sub-λ slit somewhat emphasizes the lower frequencies, as pointed out by the slight red-shift observed for the SSBCD spectrum. However, we also stress the fact that the THz waveform acquired via the SSBCD device maintains its quasi single-cycle feature (red curve in Fig. 3), thus preserving a smooth ultra-broadband frequency response extending beyond 10 THz.

B. Bias voltage and probe energy scaling mechanisms

We proceeded in our investigation studying the scaling mechanisms in the THz transients acquired via our device, as a function of both bias voltage and probe energy. Figure 4 shows the THz waveforms recorded by varying the bias voltage in the range of 5-100 V, while the probe energy was held constant at 150 nJ. As mentioned above, it results that the retrieved THz transients are quasi single-cycle with an envelope pulse duration lasting around τ_{FWHM} = 226 fs, approximatively corresponding to a bandwidth of 11 THz (see inset), for any bias voltage value. This confirms that the dispersion introduced by the sub-λ SiN cover layer does not affect the nonlinear frequency mixing and, therefore,

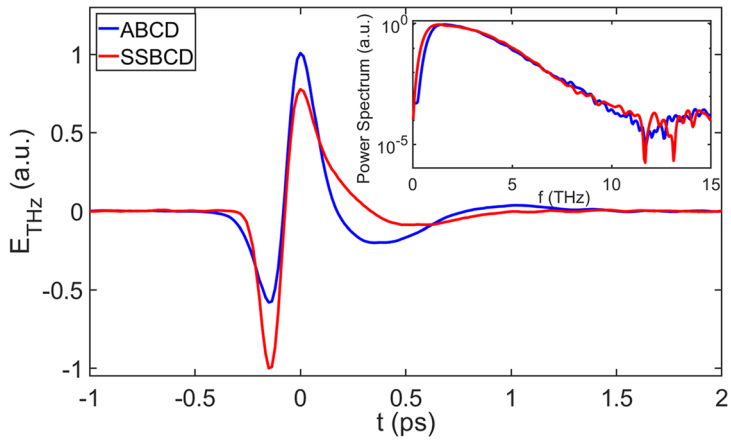

FIG. 3. Comparison between the THz waveforms recorded via ABCD (blue curve) and SiN-SSBCD (red curve). The inset shows the comparison between the Fourier-transformed spectra of the two pulses.

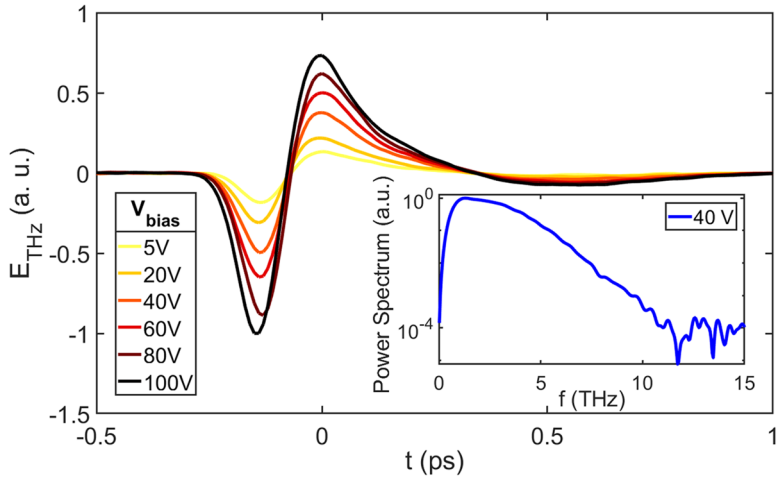

FIG. 4. THz waveforms acquired via SSBCD for different values of the bias voltage in the 5-100 V range. The inset shows the spectrum corresponding to the case of 40 V. Each curve is normalized to the (absolute) maximum value retrieved for 100 V.

the frequency response of the device. In particular, Fig. 5 illustrates the trend of the THz electric field peak as a function of the bias voltage (blue dotted line, left axis), compared to the dynamic range (DR, red dotted line, right axis). The DR is evaluated as the ratio between the THz pulse peak and the root mean square of the noise floor, and the latter is recorded when the THz pulse is absent.[31] We note that the signal, as well as the DR, is linearly proportional to the bias voltage in the whole range, as highlighted by the linear fit (black solid line). Interestingly, the monotonic DR trend is different from the behavior seen in Ref. 2, where we observed that for the very high bias voltages generated by the relatively noisy kV amplifier, the noise figure eventually worsened. On the contrary, in this case, the absence of DR deterioration is ascribed to the almost noise-free amplification of the EFISH signal operated by standard low voltage amplifiers, which allows increasing the detection efficiency without degrading the DR. We would like to underline that DRs greater than 1000 are easily reached for bias voltages of few tens of volts, while detection can be still carried out for values as low as 5 V.

Figure 6 shows the THz peak trend (blue dotted line) and the related DR (red dotted line) as a function of the probe energy in the range 10-200 nJ. Lower energy values did not allow recovering a signal out of the noise floor, whereas higher values caused permanent damage to the aluminum contact pads during long operations. It is known that in the case of pure four-wave mixing among fundamental

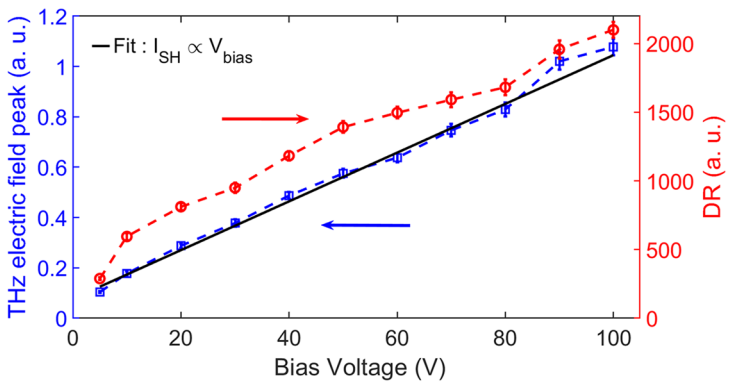

FIG. 5. THz electric field peak (blue squares, left axis) and dynamic range (red circles, right axis) trends as a function of the bias voltage. The black solid line represents the linear fit featuring the retrieved THz peak trend within the investigated bias voltage range.

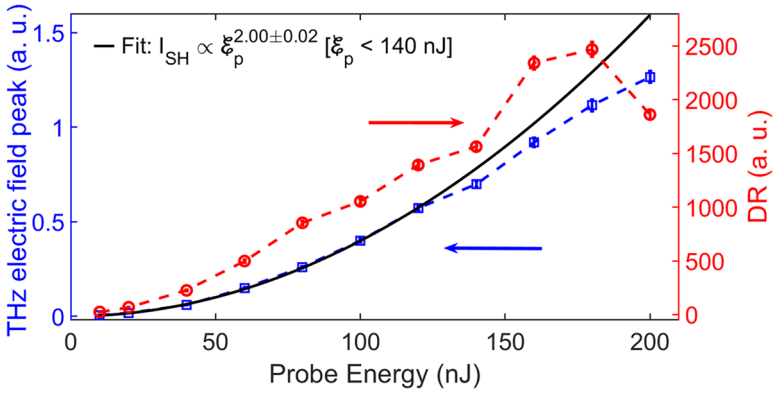

FIG. 6. THz electric field peak (blue squares, left axis) and dynamic range (red circles, right axis) trends as a function of the probe energy. The black solid line represents the parabolic fit reproducing the retrieved THz peak trend in the 10-140 nJ range.

harmonic (FH), second harmonic (SH), and THz frequencies, the SH intensity as a function of the FH energy follows a quadratic law.[32] Here, the experimental results verify such a trend for probe energies lower than 140 nJ, as highlighted by the quadratic fit (black solid line). For higher values, the data trend shows a slower increasing rate. The reason behind such a behavior is most likely the triggering of other nonlinear phenomena (e.g., nonlinear absorption, broadening of the EFISH bandwidth[33]) occurring in SiN for relatively high probe intensities. Furthermore, we report an abrupt drop of the DR when the probe pulse energy approaches 200 nJ because of a noise floor increase for such high energy values, likely due to the generation of white light in the material. Indeed, DR worsening for higher optical energies was already observed in a similar scaling mechanism underlying gas-based techniques, where the elevated probe intensity required to attain quasi-coherent detection also generated a large background noise, strongly degrading the noise figure.[34] As a final note, it is worth noticing that we were able to detect the THz signal starting from a probe energy of only 10 nJ, which is—to the best of our knowledge—the lowest ever employed for this type of coherent detection methods.

C. THz electric field peak estimation

As a further set of measurements, we used our new device as an absolute THz peak meter for ultrashort THz pulses. Indeed, the EFISH process itself occurring in the SSBCD device directly allows probing the THz electric near-field enhanced by the slit. In particular, we followed the strategy suggested in the work of Iwaszczuk *et al.*[35] We recall that when both the THz (E_{THz}) and a generic bias electric field (E_{bias}) interact with the probe beam, the total intensity of the EFISH beam is given by

$$I_{SH}^{total} \propto (E_{\mathrm{THz}})^2 + (E_{bias})^2 \pm 2E_{\mathrm{THz}}E_{bias}, \tag{1}$$

where the double sign depends on the orientation of the bias and THz electric fields, assuming a parallel polarization for both fields. In order to carry out the heterodyne detection underlying either standard ABCD or SSBCD, the bias is chosen as an AC modulated voltage wave, typically oscillating at half of the repetition rate of the pulsed THz beam and employed as a reference for the lock-in amplifier. Hence, the two squared terms in Eq. (1) are rejected, thus simplifying Eq. (1),

$$I_{SH}^{heterodyne} \propto 2E_{\mathrm{THz}}E_{bias}^{AC}. \tag{2}$$

On the other hand, if we apply a DC (i.e., static) bias field and chop the THz beam, thus acquiring the EFISH signal by synchronizing the lock-in amplifier to the same chopping frequency, only the quadratic term dependent on the bias electric field is suppressed in Eq. (1), leading to

$$I_{SH} \propto (E_{\mathrm{THz}})^2 \pm 2E_{\mathrm{THz}}E_{bias}^{DC}. \tag{3}$$

Now, if we consider two measurements carried out via the latter scheme, one with (I_{SH}^{B}) and one without (I_{SH}^{0}) a static bias voltage applied (V_{bias}^{DC}), it turns out that, from Eq. (3), the THz electric field

can be evaluated as

$$E_{\mathrm{THz}} = \frac{2E_{bias}^{DC}}{\overline{\Delta I}} \approx \frac{2V_{bias}^{DC}}{\varepsilon_{DC} d \overline{\Delta I}}, \tag{4}$$

where $\overline{\Delta I} = \left(I_{SH}^{B} - I_{SH}^{0}\right)/I_{SH}^{0}$ is the relative change of EFISH intensity. Here, we assumed that in the framework of a simple capacitor model, the bias electric field is equal to the ratio between the effective bias voltage ($V_{bias}/\varepsilon_{DC}$, being $\varepsilon_{DC} \approx 7$ the static dielectric constant of PECVD SiN[36]) and the slit width d. By means of Eq. (3), we evaluated a THz electric field peak in the slit of $E_{\mathrm{THz}}^{peak} = 141 \pm 12$ kV/cm. By considering the Fresnel losses at the interface air/SiN ($t_{Air \to SiN} = 58\%$ in terms of electric field, assuming $n_{SiN} \approx 2.45$, see the supplementary material) and the previously evaluated FE = 6.1, such a peak value is consistent with the above-mentioned THz field peak measured at the detection position (~44 kV/cm).

IV. CONCLUSION AND OUTLOOK

In conclusion, we demonstrated the ultra-broadband detection capability of a new class of SiN-based SSBCD devices operating at bias values in the order of ~10 V and probe energies of a few tens of nJ only, both being, to the best of our knowledge, the lowest ever employed in detection methods based on the EFISH mechanism. Our detector enables the possibility to operate the SSBCD technique with bias voltages switching at higher frequencies (>10 kHz), easily provided by cost-effective low voltage amplifiers. This potentially makes the SSBCD able to improve the noise performance of ultra-broadband TDS systems, thus competing with PCSs, which instead suffer from limited, notch-affected bandwidth responses (<7 THz). Moreover, the reduced probe energy opens up a new scenario of ultra-broadband applications for sources completely pumped by high repetition rate laser oscillators (<100 nJ, >1 MHz). Remarkably, such sources feature valuable beam stability and low pulse energy fluctuations, key aspects to boost the performance of low-noise portable THz systems. Finally, we envisage that a slightly revised geometry further improving the FE, together with a more efficient probe focusing scheme, could allow operating the SiN-based SSBCD devices with fiber-integrated laser oscillators.

SUPPLEMENTARY MATERIAL

See supplementary material for details regarding the simulations of the field enhancement induced by the sub-λ metallic slit.

ACKNOWLEDGMENTS

This work (for R.M. and L.R.) was supported by the Natural Sciences and Engineering Research Council of Canada (NSERC) through the Discovery and Strategic grant programs, by the Ministère de l'Économie, de la Science et de l'Innovation (MESI) of Québec and by PRIMA Quebec. A.T. thanks the Mitacs Acceleration program. R.P. acknowledges the Fonds de Recherche du Québec—Nature et Technologies (FRQNT). R.M. acknowledges further support from the ITMO Fellowship and Professorship Program (Grant No. 074-U 01) and from the 1000 Talents Sichuan Program. M.C. acknowledges support from UKRI and EPSRC (UKRI Innovation Fellowship No. EP/S001573/1 and Innovate No. UK/EPSRC EP/R043299/1). M.P. acknowledges support from EPSRC, under Grant No. EP/M013294/1. M.P. research also received funding from the EU's "Horizon 2020" research and innovation programme, GA 725046. We also thank the support from our industrial partners ACME Engineering Prod. Ltd., TeTechS Inc., Integrity Testing Inc., Lumenera Corporation, 1Qbit, and Newlight Photonics.

All relevant data present in this publication can be accessed at DOI: https://doi.org/10.5525/gla.researchdata.672.

[1] M. Tonouchi, Nat. Photonics **1**, 97 (2007).
[2] A. Tomasino, A. Mazhorova, M. Clerici, M. Peccianti, S.-P. Ho, Y. Jestin, A. Pasquazi, A. Markov, X. Jin, R. Piccoli, S. Delprat, M. Chaker, A. Busacca, J. Ali, L. Razzari, and R. Morandotti, Optica **4**, 1358 (2017).
[3] P. Y. Han and X.-C. Zhang, Meas. Sci. Technol. **12**, 1747 (2001).

[4] C.-S. Yang, C.-M. Chang, P.-H. Chen, P. Yu, and C.-L. Pan, Opt. Express **21**, 16670 (2013).
[5] J. Takayanagi, H. Jinno, S. Ichino, K. Suizu, M. Yamashita, T. Ouchi, S. Kasai, H. Ohtake, H. Uchida, N. Nishizawa, and K. Kawase, Opt. Express **17**, 7533 (2009).
[6] Z. Jiang, M. Li, and X.-C. Zhang, Appl. Phys. Lett. **76**, 3221 (2000).
[7] Y. C. Shen, P. C. Upadhya, E. H. Linfield, H. E. Beere, and A. G. Davies, Appl. Phys. Lett. **83**, 3117 (2003).
[8] N. Vieweg, B. M. Fischer, M. Reuter, P. Kula, R. Dabrowski, M. A. Celik, G. Frenking, M. Koch, and P. U. Jepsen, Opt. Express **20**, 28249 (2012).
[9] A. G. Davies, A. D. Burnett, W. Fan, E. H. Linfield, and J. E. Cunningham, Mater. Today **11**, 18 (2008).
[10] R. J. Falconer and A. G. Markelz, J. Infrared, Millimeter, Terahertz Waves **33**, 973 (2012).
[11] B. M. Fischer, M. Walther, and P. U. Jepsen, Phys. Med. Biol. **47**, 3807 (2002).
[12] M. R. Kutteruf, C. M. Brown, L. K. Iwaki, M. B. Campbell, T. M. Korter, and E. J. Heilweil, Chem. Phys. Lett. **375**, 337 (2003).
[13] I.-C. Ho, X. Guo, and X.-C. Zhang, Opt. Express **18**, 2872 (2010).
[14] C. Somma, G. Folpini, J. Gupta, K. Reimann, M. Woerner, and T. Elsaesser, Opt. Lett. **40**, 3404 (2015).
[15] C. Kübler, R. Huber, and A. Leitenstorfer, Semicond. Sci. Technol. **20**, S128 (2005).
[16] Q. Wu and X. C. Zhang, Appl. Phys. Lett. **70**, 1784 (1997).
[17] Y. Zhang, X. Zhang, S. Li, J. Gu, Y. Li, Z. Tian, C. Ouyang, M. He, J. Han, and W. Zhang, Sci. Rep. **6**, 26949 (2016).
[18] B. Ferguson and X.-C. Zhang, Nat. Mater. **1**, 26 (2002).
[19] X. Lu and X.-C. Zhang, Front. Optoelectron. **7**, 121 (2014).
[20] J. Dai, X. Xie, and X. C. Zhang, Phys. Rev. Lett. **97**, 103903 (2006).
[21] N. Karpowicz, J. Dai, X. Lu, Y. Chen, M. Yamaguchi, H. Zhao, X.-C. Zhang, L. Zhang, C. Zhang, M. Price-Gallagher, C. Fletcher, O. Mamer, A. Lesimple, and K. Johnson, Appl. Phys. Lett. **92**, 011131 (2008).
[22] C.-Y. Li, D. V. Seletskiy, Z. Yang, and M. Sheik-Bahae, Opt. Express **23**, 11436 (2015).
[23] J. Liu, J. Dai, S. L. Chin, and X.-C. Zhang, Nat. Photonics **4**, 627 (2010).
[24] K. Ikeda, R. E. Saperstein, N. Alic, and Y. Fainman, Opt. Express **16**, 12987 (2008).
[25] M. A. Seo, H. R. Park, S. M. Koo, D. J. Park, J. H. Kang, O. K. Suwal, S. S. Choi, P. C. M. Planken, G. S. Park, N. K. Park, Q. H. Park, and D. S. Kim, Nat. Photonics **3**, 152 (2009).
[26] J.-H. Kang, D.-S. Kim, and M. Seo, Nanophotonics **7**, 763 (2018).
[27] M. Shalaby, H. Merbold, M. Peccianti, L. Razzari, G. Sharma, T. Ozaki, R. Morandotti, T. Feurer, A. Weber, L. Heyderman, B. Patterson, and H. Sigg, Appl. Phys. Lett. **99**, 041110 (2011).
[28] X. Lu, R. Wan, G. Wang, T. Zhang, and W. Zhang, Opt. Express **22**, 27001 (2014).
[29] V. A. Andreeva, O. G. Kosareva, N. A. Panov, D. E. Shipilo, P. M. Solyankin, M. N. Esaulkov, P. González De Alaiza Martínez, A. P. Shkurinov, V. A. Makarov, L. Bergé, and S. L. Chin, Phys. Rev. Lett. **116**, 063902 (2016).
[30] T. Bartel, P. Gaal, K. Reimann, M. Woerner, and T. Elsaesser, Opt. Lett. **30**, 2805 (2005).
[31] M. Naftaly and R. Dudley, Opt. Lett. **34**, 1213 (2009).
[32] D. J. Cook, J. X. Chen, E. A. Morlino, and R. M. Hochstrasser, Chem. Phys. Lett. **309**, 221 (1999).
[33] M. Petev, N. Westerberg, E. Rubino, D. Moss, A. Couairon, F. Légaré, R. Morandotti, D. Faccio, and M. Clerici, Photonics **4**, 7 (2017).
[34] X. Lu, N. Karpowicz, and X.-C. Zhang, J. Opt. Soc. Am. B **26**, A66 (2009).
[35] K. Iwaszczuk, A. Andryieuski, A. Lavrinenko, X.-C. Zhang, and P. U. Jepsen, Opt. Express **20**, 8344 (2012).
[36] G. S. May and S. M. Sze, *Fundamentals of Semiconductor Fabrication* (Wiley, 2004).